Scaling and Performance of Simultaneously Heaving and Pitching Foils

Tyler Van Buren,[*] Daniel Floryan,[†] and Alexander J. Smits[‡]
Princeton University, Princeton, New Jersey 08544

The propulsive performance of an unsteady heaving and pitching foil is considered, and an extensive experimental parameter space of motion amplitudes, frequencies, and phase offsets between the heave and pitch motions is studied. The phase offset proves to be a critical parameter in determining the foil propulsive performance. To maximize thrust, the pitch motion needs to lag the heave motion by about 30 deg; but, to maximize efficiency, the lag needs to increase to about 90 deg, corresponding to a slicing motion where the angle of attack is minimized. Scaling relations are also presented, and they are developed from lift-based and added mass forces, which describe the experimental data closely. Using the scaling relations as a guide, increases in performance are found when foil amplitudes (specifically pitch) increase while maintaining a modest angle of attack.

Nomenclature

a	=	trailing-edge position
a_h^*	=	h_0/c
a_θ^*	=	θ_0
a^*	=	a/c
C_L	=	lift coefficient; C_L
C_P	=	power coefficient; $P/(1/2)\rho U_\infty^3 sc$
C_T	=	thrust coefficient; $F_x/(1/2)\rho U_\infty^2 sc$
c	=	foil chord
F_D	=	drag offset
$F_{x,y}$	=	streamwise x and lateral y force
f	=	frequency of motion
f^*	=	reduced frequency; fc/U_∞
h	=	heave position (leading edge)
L	=	lift force
M_z	=	spanwise moment
m_w	=	mass of displaced fluid in the wake
P	=	foil input power; $F_y\dot{h} + M_z\dot{\theta}$
Re	=	chord-based Reynolds number; cU_∞/ν
St	=	Strouhal number; $2fa_0/U_\infty$
St_h	=	Strouhal number based on heave, where the Strouhal number is equal to $2fh_0/U_\infty$
St_θ	=	Strouhal number based on pitch, where the Strouhal number is equal to $2fc\theta_0/U_\infty$
s	=	foil span
t	=	time
U_{eff}	=	effective velocity incoming to foil; $\sqrt{U_\infty^2 + \dot{h}^2}$
U_∞	=	freestream velocity
U^*	=	nondimensional effective velocity; $\overline{U_{\text{eff}}}/U_\infty$
u_w	=	characteristic wake velocity
α	=	angle of attack
η	=	propulsive efficiency; C_T/C_P
θ	=	pitch angle
ν	=	kinematic viscosity
ρ	=	fluid density
ϕ	=	phase angle between heave and pitch motions
ψ	=	phase angle between heave and angle-of-attack motions

Subscript

0	=	amplitude of time-varying signal

Superscripts

$\cdot$	=	first time derivative
$\cdot\cdot$	=	second time derivative
—	=	time average

I. Introduction

OVER the past 20 or 30 years, there has been considerable interest in finding new methods of propulsion for underwater vehicles that are inspired by biology [1–3]. Many fish swim by using propulsion methods where the principal thrust comes from oscillating a propulsive surface, such as a fluke or caudal fin, in a combined heave and pitch motion [4]. In many cases, a reasonably clear distinction can be made between the body as the main source of drag and the propulsor as the main source of thrust; if the body/fin interaction can be neglected, the propulsor performance may be studied separately. Here, we focus our attention on the thrust and efficiency of a foil moving in heave and pitch as a simplified model of an isolated propulsor for possible application to a new generation of underwater vehicles.

The performance of submerged foils in combined heaving and pitching motion has already been studied relatively extensively [1,2,5–7]. In a particularly influential work, Anderson et al. [8] obtained efficiencies as high as 87% using a heaving and pitching two-dimensional NACA 0012 airfoil in sinusoidal motion. They connected the wake structure to the performance of the foil, arguing that, for maximum efficiency, the leading-edge vortex pair needed to interact beneficially with the trailing-edge vorticity. In related work, Read et al. [9] recognized the importance of the peak angle of attack when considering performance, although they reported lower values of efficiency (55–70%) than the 87% reported by Anderson et al. [8] in the same laboratory under similar experimental conditions. The phase angle between the heave and pitch motions was also examined briefly, although the authors, somewhat surprisingly, did not find it to be very influential. Experiments on large-amplitude motions by Scherer [10] showed similar peak efficiency values to those found by Read et al. [9] over a wide range of parameters.

In terms of optimization, Kaya and Tuncer [11] numerically studied heaving and pitching airfoil performance in laminar air flow, and they used gradient-based optimization of the motion paths to show that there were significant benefits to thrust by moving nonsinusoidally. They found that motions that maintained a constant angle of attack for longer periods of time, which was a topic also

considered by Read et al. [9], produced higher thrust than purely sinusoidal motions.

The theory of heaving and pitching plates and foils has a long history. Theodorsen [12] first derived the linearized expressions for the forces generated by an oscillating foil in 1935 in the context of aerodynamic flutter. His analysis included the contributions due to aerodynamic (circulation-based) forces and added mass forces. Garrick [13] used Theodorsen's [12] results to develop expressions for thrust and power for a two-dimensional rigid propulsor, and Lighthill [5] used Garrick's [13] results to estimate the forces produced by the lunate tail of a fish in the context of his elongated-body theory, which he later extended to large-amplitude motions [14] (although only added mass forces were considered in the latter work). Chopra [15] and Chopra and Kambe [16] extended Lighthill's [14] work to three dimensions by incorporating the lifting-line theory, and Wu [17] considered the performance of a flexible foil with a prescribed deformation. Then, Katz and Weihs [18] were the first to consider the addition of chordwise flexibility on a two-dimensional foil where the structural mechanics were coupled to the fluid mechanics.

What appears to be missing in the literature is a generic scaling analysis for heaving and pitching foils that embodies the possibly nonlinear underlying physical mechanisms that generate thrust and determine efficiency. In this respect, Floryan et al. [19] combined unsteady lift [12] and added mass forces [20] to construct scaling relations that described the mean forces generated by heaving or pitching foils. They showed that the mean thrust generated by heaving motions was entirely lift based, whereas the mean thrust generated by pitching motions was from added mass alone. In contrast, for heave and pitch, the mean input power (and thus efficiency) depended on both lift-based and added mass forces. These scaling relations have since been extended to intermittent motions by accounting for the duty cycle of the motion [21], as well as to nonsinusoidal motions by adding a parameter based on the peak trailing-edge velocity of the foil [22].

Here, we extend the approach of Floryan et al. [19] to derive scaling relationships for foils that are simultaneously heaving and pitching. We verify the relationships against experiments covering a large range of heave and pitch amplitudes, frequencies, and phase differences. This approach allows us to pinpoint physical mechanisms that influence thrust and efficiency, which can then be used as a guide to improve performance.

II. Experimental Methods

Experiments on a simultaneously heaving and pitching foil were conducted in a free-surface recirculating water tunnel with a $0.46 \times 0.3 \times 2.44$ m test section and baffles to minimize surface waves. The tunnel velocity was fixed at a constant value of $U_\infty = 0.1$ m/s. The experimental setup is illustrated in Fig. 1.
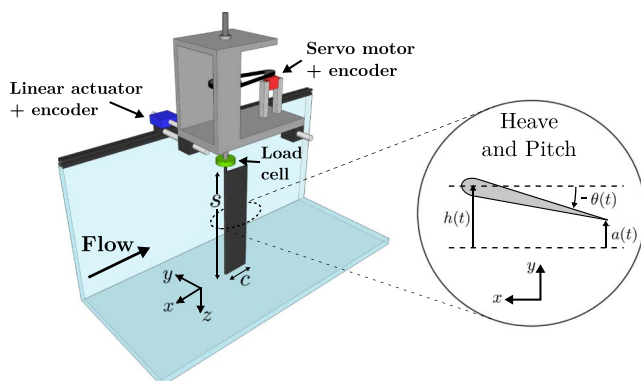
Table 1 Experimental parameter space

Parameter	Range
Freestream velocity	$U_\infty = 0.1$ m/s
Chord	$c = 80$ mm
Span	$s = 279$ mm
Frequency	$f = 0.2, 0.3, \ldots, 0.8$ Hz
Heave amplitude	$h_0 = 10, 20, 30$ mm
Pitch amplitude	$\theta_0 = 5, 10, 15$ deg
Phase offset	$\phi = 0, 30, \ldots, 210, 220, \ldots, 330$ deg

A teardrop foil was used with a chord $c = 80$ mm, a maximum thickness of 8 mm, and a span $s = 279$ mm, yielding a chord-based Reynolds number of $Re = 8000$. Heave motions were generated by a linear actuator (Linmot PS01-23 × 80F-HP-R) pushing the foil carriage on near-frictionless air bearings (NewWay S301901), and pitch motions about the leading edge were generated by a servo motor (Hitec HS-8370TH). Both motions were simultaneously measured via encoders. The foil was actuated sinusoidally according to

$$ h = h_0 \sin(2\pi f t), \quad \theta = \theta_0 \sin(2\pi f t + \phi) \tag{1} $$

at frequencies $f = 0.2$ to 0.8 Hz every 0.1 Hz, with heave amplitudes of $h_0 = 10$, 20, and 30 mm; pitch amplitudes $\theta_0 = 5$, 10, and 15 deg; and phase differences $\phi = 0$ to 330 deg in intervals of 30 deg, with a more refined spacing of 10 deg between 210 and 330 deg (see Table 1 and Fig. 2). Altogether, the parameter space comprised 1260 unique cases.

The forces and moments of the foil were measured using a six-component sensor (ATI Mini40), with force and torque resolutions of 5×10^{-3} N and 1.25×10^{-4} N · m, respectively, in the x and y directions and 10^{-2} N and 1.25×10^{-4} N · m in the z direction, sampled at 100 Hz. Each case ran for 30 cycles of the motion, with the first and last five cycles used for warmup and cooldown. Before every case, we zeroed the force sensor to minimize any voltage drift. Due to the sufficient repeatability shown by similar experiments in the past [19,21,22], only one trial of each case was performed.

III.   Results and Discussion

The results on propulsive performance are presented in terms of the nondimensional thrust coefficient, input power coefficient, and Froude efficiency defined by

$$ C_T = \frac{F_x}{(1/2)\rho U_\infty^2 sc}, \quad C_P = \frac{F_y \dot{h} + M_z \dot{\theta}}{(1/2)\rho U_\infty^3 sc}, \quad \eta = \frac{C_T}{C_P} \tag{2} $$

Fig. 1   Experimental setup and motion definition.
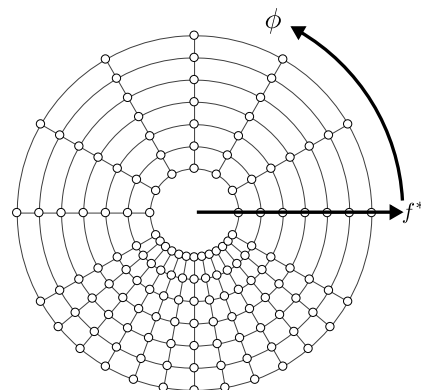

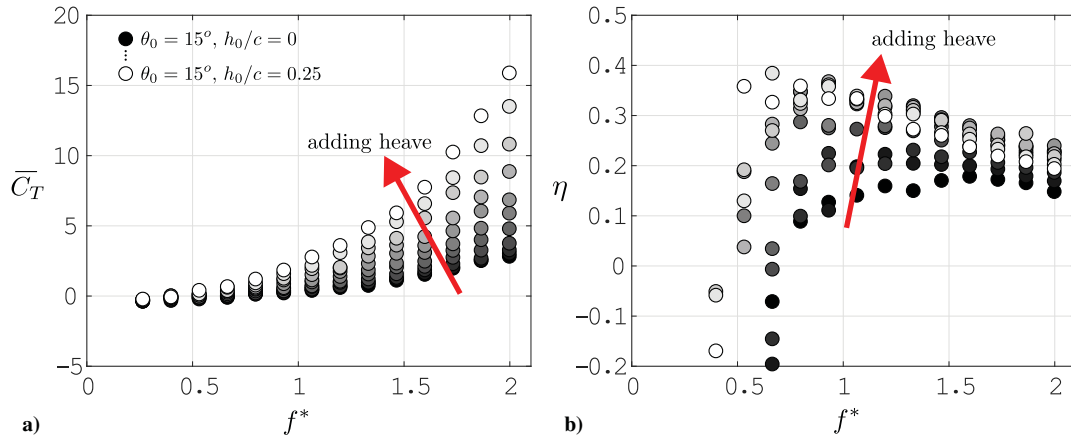**Fig. 2   Diagram depicting the parameter space on a frequency-phase plot.**

Fig. 3   Time-averaged a) thrust coefficient and b) efficiency of a pitching foil with incremental increases in heave amplitude.

We denote the time-averaged values of these parameters by $\bar{C}_T$ and $\bar{C}_P$, respectively, whereas efficiency is always reported as a time-averaged quantity. The foil kinematics are characterized by the Strouhal number $St = 2fa_0/U_\infty$, where a_0 is the peak amplitude of the trailing-edge motion, and by the reduced frequency $f^* = fc/U_\infty$.

To illustrate the effects of combining heave and pitch motions, Fig. 3 displays the time-averaged thrust coefficient and efficiency of a pitching foil with incremental increases in heave amplitude, at a phase offset of $\phi = 270$ deg, while keeping the pitch amplitude fixed at $\theta_0 = 15$ deg. The results shown in Figs. 3a and 3b are from an additional dataset not shown in Table 1 where $U_\infty = 60$ mm/s, $f = 0.2, 0.3, \ldots, 1.5$ Hz, and $h_0 = 0, 2, \ldots, 20$ mm. In this case, adding heave to the pitching motion increases thrust and efficiency significantly. Note also that the efficiency curves exhibit a maximum value, indicating that there is an optimum efficiency point. For low values of f^*, the efficiency decreases sharply as the effects of the viscous drag on the propulsor become important. For high values of f^*, the efficiency approaches its inviscid or ideal value, which slowly decreases with increasing reduced frequency. The beneficial effects of combining pitching and heaving motions were first discussed by von Kármán and Burgers [23] and more recently recapitulated by Wu [3].

A.   Maximizing Performance Through Combined Motion

When combining sinusoidal heaving and pitching motions, the phase offset becomes a critical parameter. Figure 4 illustrates the motion of a swimming foil for phase differences of $\phi = 0, 90, 180,$ and 270 deg. When heave and pitch are in phase, the motion appears to an observer moving with the foil as if the foil is pitching about some

point upstream of the leading edge. For phase angles around $\phi = 90$ deg, the trailing edge leads the leading edge. When $\phi = 180$ deg, the foil appears to pitch about a point behind the leading edge. However, $\phi = 270$ deg seems to be the most "fishlike," cleanly slicing through the water with the lowest angles of attack (represented by the angle between the foil and its instantaneous direction of motion).

To appreciate the importance of pitch angle in producing thrust, we first consider how thrust is generated by heave-only motions, as shown in Fig. 5a. Thrust production in heave is lift based, meaning that the lateral velocity of the foil $\dot{h}$ combines with the freestream velocity U_∞ into an effective foil velocity U_{eff} that produces lift L. Because the lift vector is perpendicular to the effective velocity vector, L has components in the lateral and streamwise directions (F_y and F_x, respectively), with the latter being the thrust. To produce thrust efficiently, we need to avoid dynamic stall; thus, we need to limit the maximum angle of attack α. To produce higher thrust, however, we need to increase the heave velocity, which will then increase the angle of attack.

This conflict can be mitigated by adding pitch to the heave motion such that the angle of attack is reduced. Consider a heaving foil with fishlike pitching motion added ($\phi = 270$ deg), as shown in Fig. 5b. Compared to heave-only motions (Fig. 5a), the heave velocity is greater but the angle of attack is the same due to the addition of appropriate pitch. The increased heave velocity increases the lift and rotates more of it in the thrust direction, increasing the efficiency. Thus, the phase difference between the heave and pitch motions is a crucial factor in determining the foil performance.

Figure 6 shows the time-averaged output performance (thrust, power, and efficiency) for all the phases and frequencies tested at heave and pitch amplitudes of $h_0/c = 0.375$ and $\theta_0 = 15$ deg, respectively. In each subfigure, the phase difference ϕ varies in the azimuthal direction, whereas the reduced frequency f^* varies in the radial direction. Note that these trends are representative of all of the combinations of heave and pitch amplitudes tested in this study, and that the full results are presented in Appendix A.

The Strouhal number St and trailing-edge amplitude a_0^* are largest for $\phi = 0$ deg because in-phase heave and pitch motions will result in the greatest peak-to-peak excursion of the trailing edge. The peak angle of attack α_0, however, aligns with $\phi = 90$ deg. Interestingly, the thrust does not follow the behavior of the Strouhal number, which would be expected if the Strouhal number was the sole governing parameter for these flows, as suggested in [24]. The peak thrust actually occurs around $\phi \approx 330$ deg, where the trailing edge of the foil lags the leading edge by 30 deg. Conversely, the peak power is tilted toward $\phi \approx 30$ deg. The peak efficiency occurs around $\phi = 270$ deg, which is coincident with the smallest peak angles of attack. This observation agrees with other researchers who have argued that the peak angle of attack is an important performance parameter [8,11], with the former study specifically using
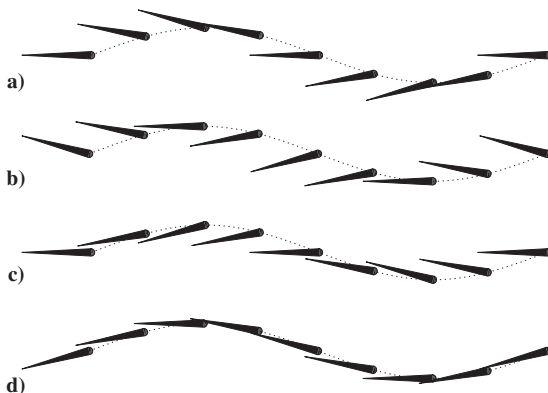

Fig. 4   Motion of a foil swimming from left to right via heave and pitch motions with a phase offset: a) $\phi = 0$ deg, b) 90 deg, c) 180 deg, and d) 270 deg.
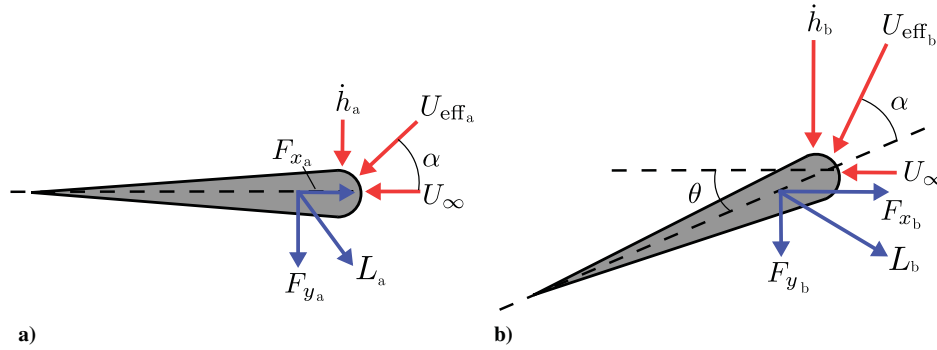
Fig. 5   Heaving foil a) without and b) with added pitch motion. Streamwise, heave, and effective velocities are shown in red; and resulting lift-based forces are shown in blue.
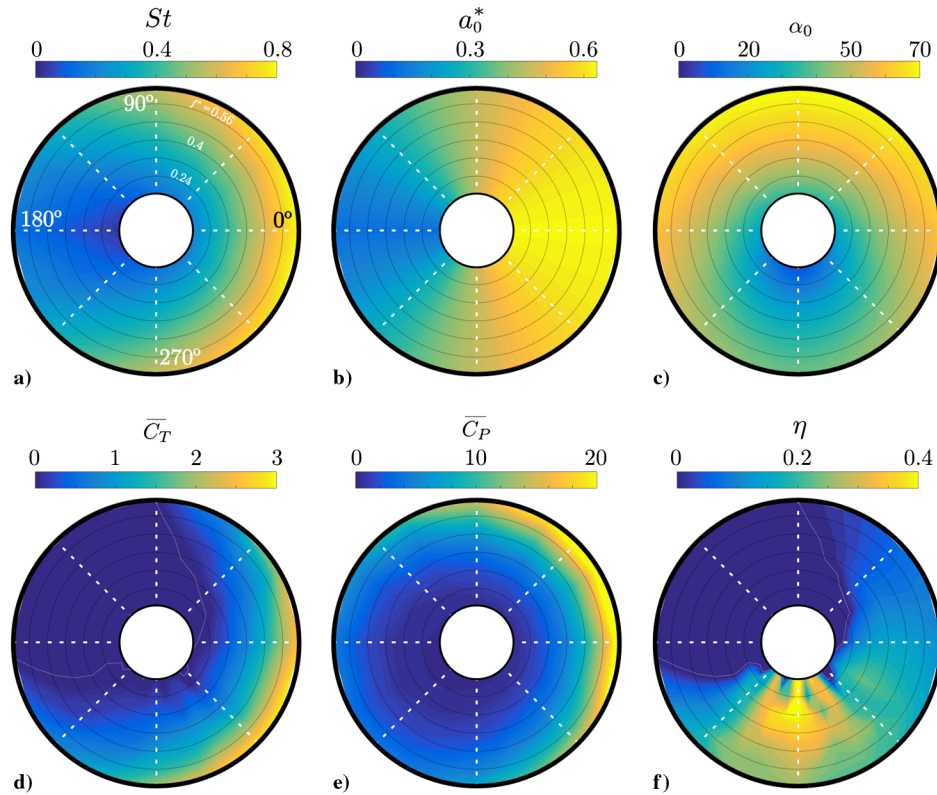

Fig. 6   Impact of phase offset (ϕ, shown in the azimuthal variation) and reduced frequency (f^*, shown in the radial direction) on a) Strouhal number; b) amplitude-to-chord ratio; c) peak angle of attack; d) time-averaged thrust coefficient; e) time-averaged power coefficient; and f) efficiency. Heave amplitude-to-chord ratio is $h_0/c = 0.375$, and pitch amplitude is $\theta_0 = 15$ deg. Reduced frequency increases radially outward, with lines marking levels at $f^* = 0.16, 0.24, \ldots, 0.64$.

$\phi = 270$ deg to achieve the highest efficiencies. We will explore this further in Sec. III.B.

The impact of phase offset can be seen more clearly in Fig. 7, which shows the same data displayed in Fig. 6 but for a fixed reduced frequency of $f^* = 0.64$. The peak thrust and minimum power occur when $\phi = 330$ and 210 deg, respectively, and the peak efficiency is almost exactly in between at $\phi = 270$ deg. Note that we do not see positive thrust for 90 deg $< \phi <$ 180 deg, even at the highest frequency and largest motion amplitudes, indicating that this range of phase offsets is of no value propulsively.

To better understand the input power behavior shown in Fig. 7, we split the power into its lateral force $F_y \dot{h}$ and moment $M_z \dot{\theta}$ components. Figure 8 shows the relative contributions of the lateral force and moment to the power over one actuation cycle for phase offsets of $\phi = 0$ and 270 deg. The contributions of the lateral force are similar for both cases, but the moment components differ markedly. When the heave and pitch motions are in phase
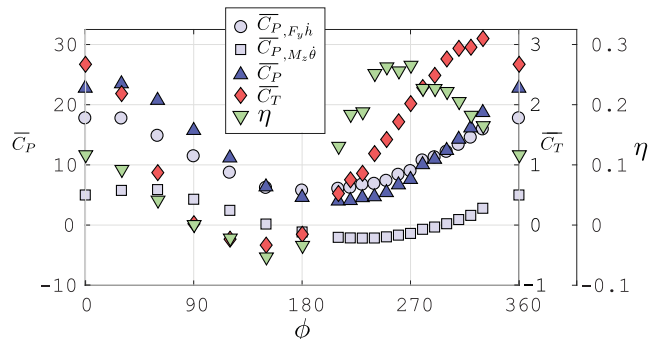

Fig. 7   Time-averaged power coefficients (force component, moment component, and total), thrust coefficient, and efficiency as they vary with phase between heave and pitch motions. The heave amplitude-to-chord ratio is $h_0/c = 0.375$, pitch amplitude is $\theta_0 = 15$ deg, and reduced frequency is $f^* = 0.64$.
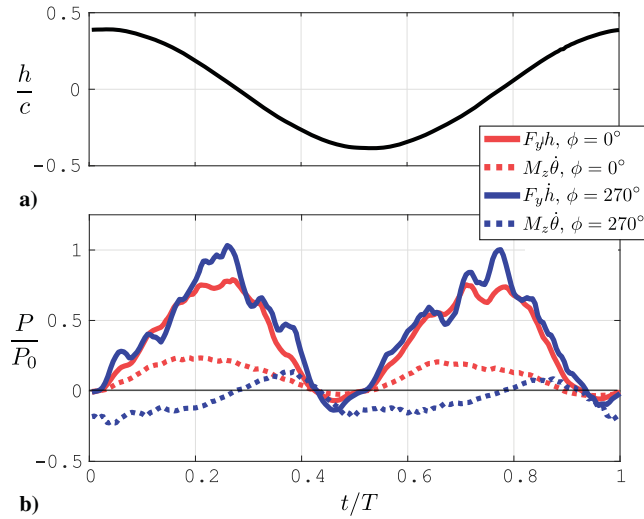
Fig. 8   Phase-averaged cycles of a) heave-to-chord ratio and b) force $F_y \dot{h}$ and moment $M_z \dot{\theta}$ components of power for $\phi = 0$ deg (red) and 270 deg (blue).

($\phi = 0$ deg), their accelerations are in phase. Thus, when the foil starts to accelerate laterally, it also accelerates rotationally in the same direction, working against the resistance of the fluid and yielding a high moment component in the power. However, when heave and pitch are offset by $\phi = 270$ deg, the lateral acceleration of the foil produces a force that assists the force associated with pitch rotation, thus lowering the moment required. This interaction between the lateral force and moment components of the input power is critical to achieving the high efficiency we see at $\phi = 270$ deg.

In summary, we find that the most efficient motions are when $\phi = 270$ deg, where the trailing edge lags the leading edge in a slicing motion. In contrast, the highest thrust motions occur when the heaving and pitching motions are nearly in phase, although this comes with a significant loss in efficiency. Note that our experimental results differ from those predicted using linear theory [13], which indicates that thrust is maximized when heave and pitch are in phase, and efficiency is maximized for phases around 225 deg. The discrepancy between our experiments and the linear theory motivates us to develop scaling laws that can explain our observations.

B.   Scaling Laws

Here, we develop a scaling analysis by considering the forces acting on the foil due to added mass and lift-based sources. We do not include the forces from the inertia of the foil, as was done in [10], because their time-averaged contributions were zero for these types of heaving and pitching flows, as shown in [25]. We base our scaling analysis on the work by Floryan et al. [19], who considered heaving and pitching motions independently.

We only consider pitching motions about the leading edge, although, as Lighthill [5] pointed out, changing the pitch axis is equivalent to changing the phase angle between the heaving and pitching motions (for small motions). We will use the $\sim$ symbol to indicate that one quantity scales as another (for example, $F = ma$ for constant mass is $F \sim a$), and we use the $\approx$ symbol to indicate one quantity is approximately equal to another (for example, $1.013 \approx 1$). In our initial analysis, we will adopt a loose notation where we intentionally ignore all multiplicative constants (such as π), but our final expressions for thrust and power will contain multiplicative constants that will need to be determined empirically. Throughout the analysis, we make a small angle approximation on the pitch angle.

First, we consider the lift-based (circulatory) forces as in the work of Theodorsen [12]. The lift force scales as $\sim \rho s c U_{\text{eff}}^2 C_L$ where the lift coefficient $C_L \sim \alpha + \dot{\alpha} c / U_{\text{eff}}$. Projecting the lift force into the

streamwise and lateral directions (multiplying by $\dot{h}/U_{\text{eff}}$ and U_∞/U_{eff}, respectively) gives

$$F_{x,L} \sim \rho s c (\underbrace{\alpha \dot{h} U_{\text{eff}}}_{1} + \underbrace{c \dot{\alpha} \dot{h}}_{2}),$$

$$F_{y,L} \sim \rho s c (\underbrace{\alpha U_\infty U_{\text{eff}}}_{1} + \underbrace{c \dot{\alpha} U_\infty}_{2})$$

where groups 1 and 2 are the steady and unsteady portions of the lift, respectively. The resulting moment about the leading edge is

$$M_{z,L} \sim \rho s c^2 U_{\text{eff}} (\alpha U_{\text{eff}} + c \dot{\alpha})$$

The angle of attack is exactly $\alpha = -\theta - \arctan(\dot{h}/U_\infty)$; however, for heave velocities on the order of the freestream velocity or less, we approximate this as $\alpha \approx -\theta - \dot{h}/U_\infty$. At this point, we choose to leave lift force terms as functions of α and not $\{\theta, h\}$ to more directly keep track of lift-based phenomena.

Next, we consider the streamwise and lateral components of the added mass forces, following the analysis of Sedov [20] and its interpretation in [19]. This yields

$$F_{x,AM} \sim \rho s c^2 (\underbrace{c \ddot{\theta} \theta + \ddot{h} \theta}_{1} + \underbrace{\dot{h} \dot{\theta}(1 + \theta^2) + \dot{\theta} \theta U_\infty}_{2} + \underbrace{c \dot{\theta}^2}_{3}),$$

$$F_{y,AM} \sim \rho s c^2 (\underbrace{c \ddot{\theta} + \ddot{h}}_{1} + \underbrace{\dot{h} \dot{\theta} \theta + \dot{\theta}(1 + \theta^2) U_\infty}_{2} + \underbrace{c \dot{\theta}^2 \theta}_{3})$$

where group 1 terms are forces arising from the foil accelerations, group 2 terms are Coriolis forces, and group 3 terms are centrifugal forces. The moment about the leading edge due to added mass is

$$M_{z,AM} \sim \rho s c^2 (c^2 \ddot{\theta} + c \ddot{h} + \dot{h}(1 + \theta^2) U_\infty + \theta U_\infty^2 + \dot{h}^2 \theta)$$

Note that $1 + \theta^2$ is on the order of $\mathcal{O}(1 + \theta_0^2)$, so we will make the approximation that $1 + \theta^2 \approx 1$.

Combining the contributions from added mass and lift yields the following expression for total thrust:

$$F_x \sim \rho s c (\alpha \dot{h} U_{\text{eff}} + c \dot{\alpha} \dot{h} + c^2 \ddot{\theta} \theta + c \ddot{h} \theta + c \dot{h} \dot{\theta} + \underline{c \dot{\theta} \theta U_\infty} + c^2 \dot{\theta}^2) - F_D \tag{3}$$

where F_D is the fluid drag force on the foil. Similarly, combining the contributions from added mass and lift for the power $P (= F_y \dot{h} + M_z \dot{\theta})$ yields

$$P \sim \rho s c (\alpha \dot{h} U_{\text{eff}} U_\infty + c \dot{\alpha} \dot{h} U_\infty + c \alpha \dot{\theta} U_{\text{eff}}^2 + c^2 \dot{\alpha} \dot{\theta} U_{\text{eff}} + c^2 \dot{h} \ddot{\theta} + \underline{c \ddot{h} \dot{h}} \\ + c \dot{h}^2 \theta \dot{\theta} + c \dot{h} \dot{\theta} U_\infty + c^2 \dot{h} \dot{\theta}^2 \theta + \underline{c^3 \dot{\theta} \ddot{\theta}} + c^2 \ddot{h} \dot{\theta} + \underline{c \theta \dot{\theta} U_\infty^2}) \tag{4}$$

In Eqs. (3) and (4), we underline terms that are inherently out of phase for a linear system with sinusoidal motions; hence, we would expect them to be small. However, Liu et al. [26] showed that there may be important nonlinearities in these types of flows, and therefore Floryan et al. [19] included these out-of-phase terms in their analysis; thus, we also retain them here.

Next, we impose sinusoidal motions for heaving and pitching, where pitch has a phase offset ϕ from the heave motion, which results in a sinusoidal variation of angle of attack with phase ψ:

$$h = h_0 \sin(2\pi f t), \quad \theta = \theta_0 \sin(2\pi f t + \phi),$$

$$\alpha = \alpha_0 \sin(2\pi f t + \psi)$$

where

$$\alpha_0 = \sqrt{\theta_0^2 + 4\pi\theta_0 \sin\phi\left(\frac{fh_0}{U_\infty}\right) + 4\pi^2\left(\frac{fh_0}{U_\infty}\right)^2} \qquad (5)$$

and

$$\psi = \arctan\left(\frac{\alpha_0 \sin\psi}{\alpha_0 \cos\psi}\right) = \arctan\left(\frac{-\theta_0 \sin\phi - 2\pi(fh_0/U_\infty)}{-\theta_0 \cos\phi}\right) \quad (6)$$

To obtain time-averaged quantities, we apply these motion functions to Eqs. (3) and (4) and integrate with respect to time over one motion cycle. The resulting time-averaged expressions for thrust and power are

$$\frac{\overline{F_x}}{\rho sc} \sim f\alpha_0 h_0 \sin\psi \overline{U_{eff}} + cf^2\alpha_0 h_0 \cos\psi + c^2 f^2\theta_0^2 + cf^2 h_0\theta_0 \cos\phi$$
$$+ cf\theta_0^2 U_\infty - \frac{\overline{F_D}}{\rho sc} \qquad (7)$$

$$\frac{\bar{P}}{\rho sc} \sim f\alpha_0 h_0 \sin\psi \overline{U_{eff}} U_\infty + cf\alpha_0\theta_0 \sin(\psi-\phi)\overline{U_{eff}}^2$$
$$+ cf^2\alpha_0 h_0 \cos\psi U_\infty + cf^2\alpha_0\theta_0 \cos(\psi-\phi)\overline{U_{eff}}$$
$$+ c^2 f^3 h_0\theta_0 \sin\phi + cf^3 h_0^2 + cf^2 h_0\theta_0 \cos\phi U_\infty$$
$$+ c^3 f^3\theta_0^2 + cf\theta_0^2 U_\infty^2 + c^2 f^3 h_0\theta_0^3 \sin\phi + cf^3 h_0^2\theta_0^2 \sin\phi \cos\phi \qquad (8)$$

We will neglect the last two terms in the power because they are of higher order and their influence will be small. The quantity $\overline{U_{eff}}$ is the time average of the effective velocity of the foil U_{eff}. It is given by the complete elliptic integral of the second kind $E[\cdot]$:

$$\overline{U_{eff}} = \frac{2U_\infty}{\pi} E\left[-\left(\frac{2\pi fh_0}{U_\infty}\right)^2\right]$$

For our range of data, $\overline{U_{eff}}$ may be approximated by

$$\overline{U_{eff}} \approx U_\infty \sqrt{1 + 2\pi^2\left(\frac{fh_0}{U_\infty}\right)^2}$$

Nondimensionalizing yields the following thrust and power coefficients:

$$\overline{C_T} \sim \underbrace{\alpha_0 St_h U^* \sin\psi}_{1} + \underbrace{\alpha_0 f^* St_h \cos\psi}_{2} + \underbrace{St_\theta^2}_{3} + \underbrace{St_h St_\theta \cos\phi}_{4}$$
$$+ \underbrace{St_\theta a_\theta^*}_{5} - \underbrace{a_\theta^*}_{6} \qquad (9)$$

$$\overline{C_P} \sim \alpha_0 St_h U^* \sin\psi + \alpha_0 St_\theta U^{*2} \sin(\psi-\phi) + \alpha_0 f^* St_h \cos\psi$$
$$+ \alpha_0 f^* St_\theta U^* \cos(\psi-\phi) + f^* St_h St_\theta \sin\phi + f^* St_h^2$$
$$+ St_h St_\theta \cos\phi + f^* St_\theta^2 + St_\theta a_\theta^* \qquad (10)$$

where $St_h = 2fh_0/U_\infty$ and $St_\theta = 2fc\theta_0/U_\infty$ are the Strouhal numbers of the heave and pitch motions individually, $f^* = fc/U_\infty$ is the reduced frequency, $a_h^* = h_0/c$ and $a_\theta^* = \theta_0$ are the amplitude to chord ratios, and $U^* = \overline{U_{eff}}/U_\infty$. We expressed the drag term $\overline{C_D}$ as a linear function of pitch amplitude θ_0: that is, a linear function of the projected frontal area for slow motions ($f \to 0$). As shown in Appendix B, this is a fair approximation for our data.

For thrust [Eq. (9)], terms 1 and 2 represent the contributions due to steady and unsteady aerodynamic lift, respectively; term 3 is partly due to foil acceleration and partly due to centrifugal force; term 4 is partly foil acceleration and partly Coriolis force; term 5 is the Coriolis force; and term 6 is the viscous drag. In the special cases of pure heave ($\theta_0 = 0$) and pure pitch ($h_0 = 0$), our expressions for thrust and power reduce to those given by Floryan et al. [19].

We now make some simplifications. First, we recognize that $\alpha_0 \cos\psi = -\theta_0 \cos\phi$ and $\alpha_0 \sin\psi = -\theta_0 \sin\phi - 2\pi fh_0/U_\infty$. Second, wherever it is possible, we combine terms into the total motion Strouhal number $St = 2fa_0/U_\infty$ where $a = h + c\theta$, thus $St^2 = St_h^2 + St_\theta^2 + 2St_h St_\theta \cos\phi$. Third, we assume that $U^* \approx 1$. Although this particular approximation may seem aggressive, changes in U^* are relatively small when compared to other input parameters like Strouhal number St, f^*, or a^*; and our results indicate that inclusion of U^* has a minor impact on the scaling. The final expressions for the thrust and power coefficients are as follows:

$$\overline{C_T} = c_1 St^2 + c_2 St_h a_\theta^* \sin\phi + \underline{c_3 St_\theta a_\theta^*} - c_4 a_\theta^* \qquad (11)$$

$$\overline{C_P} = c_5 St^2 + c_6 f^* St_h St_\theta \sin\phi + c_7 St_h a_\theta^* \sin\phi + \underline{c_8 f^* St_h^2}$$
$$+ \underline{c_9 f^* St_\theta^2} + \underline{c_{10} St_\theta a_\theta^*} \qquad (12)$$

where we have now introduced coefficients c_n to each term to account for the multiplicative constants that have been ignored in our analysis so far. These coefficients are determined via linear regression over the entire experimental dataset. Note that the value of the coefficients may depend on the airfoil shape, and they can be more specifically tuned for a fixed phase angle ϕ (we find that coefficients found by linear regression for a single ϕ are similar to the coefficients found by linear regression of the entire dataset). As before, the underlined terms are due to terms that are out of phase in a system with sinusoidal motions and would be neglected in a linearized analysis.

The experimental data for all motion amplitudes and phases, plotted as a function of these scaling relations, are shown in Fig. 9, thrust constants: $c_1 = 4.84$, $c_2 = -5.96$, $c_3 = -2.82$, and $c_4 = 0.48$. Power constants: $c_5 = 25.1$, $c_6 = 32.1$, $c_7 = 4.95$, $c_8 = 41.35$, $c_9 = 14.98$, and $c_{10} = -25.77$. For both thrust and power, we see a collapse of the data, indicating that our simplified model closely describes the propulsive performance for these types of foil motions. We see the expected linear relationship between the model thrust and the data, but the power shows a slight nonlinear behavior (also seen in [19]). To make the power scaling linear, we need to add a higher-order term (one in St^3), but that is beyond the level of the current analysis.

In Eqs. (11) and (12), the phase differences that cause out-of-phase terms (underlined in the equation) to be important may be due to the influence of the wake on the foil. Scherer [10] explained that the induced velocity of the wake on the foil changed the instantaneous angle of attack, and therefore the lift force; and it changed the inertial forces from added mass, which was equivalent to a time lag on the circulatory forces in the linearized theory (for a nonlinear system, this equivalency cannot be made [26]). We find the heave-based term in the power $f^* St_h^2$, which originates from the $\ddot{h}\dot{h}$ term in Eq. (4), to make an important contribution to the power. However, we also find that the pitch-based terms in the thrust and power (associated with constants c_3, c_9, and c_{10}) can be neglected without much penalty on the data collapse. Such terms are all of the order $\mathcal{O}(\theta_0^2)$, so this result is not surprising.

Figure 10 shows the performance maps of efficiency versus mean thrust with contours of pitch angle, peak angle of attack, and reduced frequency for multiple heave amplitudes, calculated from Eqs. (11) and (12). When creating these performance maps, we neglected the drag term in the thrust in order to calculate "ideal" efficiencies; that is, we removed the effect where efficiency rapidly decays at low reduced frequency (see Fig. 3
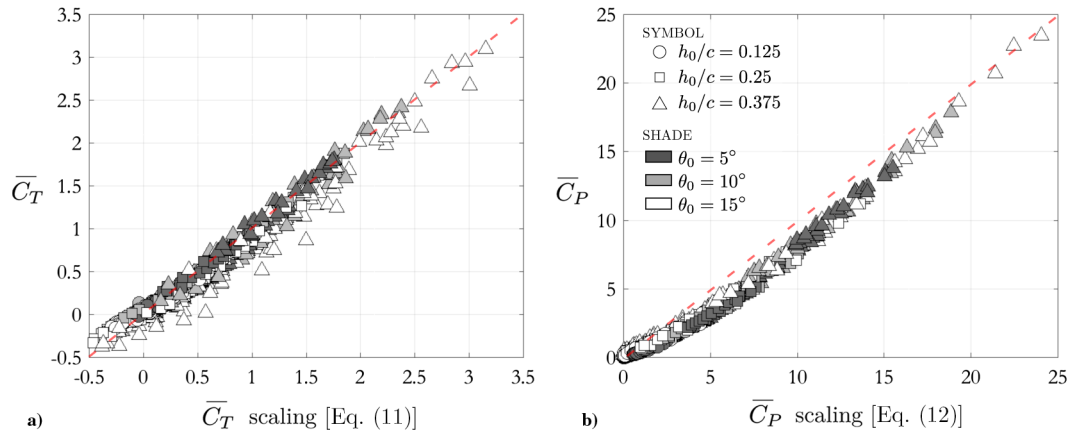
a)   b)

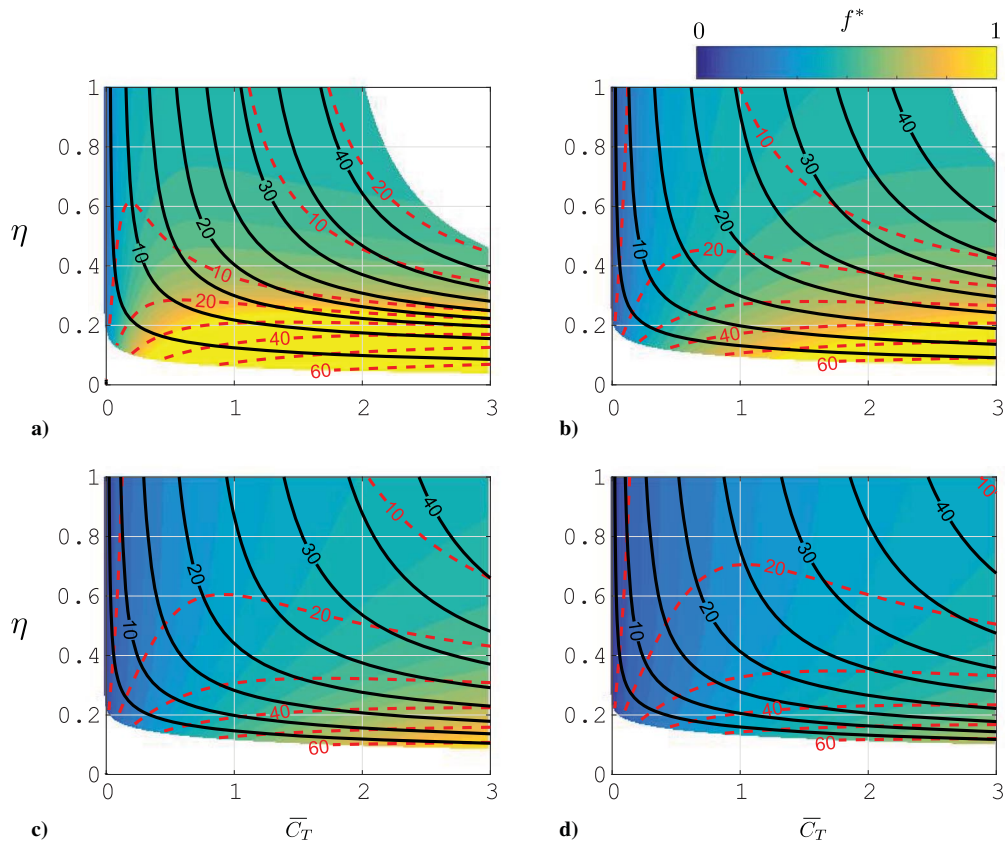**Fig. 9   Scaling of the time-averaged a) thrust and b) power coefficients for all motion amplitudes and phases tested (see Table 1).**

a)   b)

c) $\overline{C}_T$ d) $\overline{C}_T$

Fig. 10   Performance maps of efficiency and time-averaged thrust coefficient for a heaving and pitching foil with phase offset of $\phi = 270$ deg. Contours of the pitch amplitude (black solid lines) and peak angle of attack (red dashed lines) are superimposed on a color contour of reduced frequency. The heave amplitude-to-chord ratios are a) $h_0/c = 0.125$, b) 0.25, c) 0.375, and d) 0.5. They are calculated from Eqs. (11) and (12), with constants from Fig. 9.

and the accompanying discussion). The maps extend a good deal beyond our experimental dataset; although we cannot validate these extrapolated regions (especially where our approximations break down), they may be useful in identifying trends and regions that should be explored further. The regions of Figs. 10a and 10b in the upper right corner are white because our simulations did not extend that far in θ, and the bottom portions of all subfigures are white because this was the performance for the heave-only motion; thus, data cannot exist below it. Propulsors that produce high thrust and do so efficiently appear

in the top-right corner of the performance maps, so this is where propulsors should operate. There are two standout trends: for fixed motion amplitudes, decreasing the peak angle of attack increases efficiency (similar behavior seen in [11]); and for fixed frequency and heave amplitude, increasing the pitch amplitude increases both efficiency and thrust. In other words, bigger, slower motions improve efficiency as compared to smaller, faster motions.

The discussion by Alexander [27] illuminated why this is so. For unsteady propulsion, the thrust is equal to the rate at which

streamwise momentum is added to the wake $u_w \dot{m}_w$, where m_w is the mass of water that is accelerated from rest to velocity u_w. The same thrust can be generated by accelerating a small mass of water to a high velocity (small, fast motions) or a large mass of water to a low velocity (big, slow motions). The power that the system has to expend in order to overcome the body drag D during steady swimming at a velocity U_∞ is the product of drag and speed; that is, $D U_\infty = u_w \dot{m}_w U_\infty$. We think of this as the useful power. The total power expended by the system includes the useful power and the power lost to the wake, which is equal to the rate at which the kinetic energy of the wake is increased: $(1/2) u_w^2 \dot{m}_w$. The efficiency of the system is the ratio of the useful to total power, and so

$$\eta = \frac{U_\infty}{U_\infty + (1/2) u_w}$$

This simple analysis suggests that, for more efficient motions, it is desirable to minimize u_w/U_∞. For a given thrust, big, slow motions should be more efficient than small, fast motions.

IV. Conclusions

A heaving and pitching teardrop foil was studied experimentally in an effort to understand its thrust and efficiency behavior. Combining heave and pitch motions generally achieves improved performance as compared to heave or pitch in isolation, as found in previous work. A critical parameter was the phase difference between the heave and pitch motions. Peak thrust occurred near $\phi = 330$ deg, and the minimum power occurred near $\phi = 210$ deg. The peak efficiency occurred near $\phi = 270$ deg, where the smallest peak angles of attack occurred. At this most efficient phase angle, it was found that the

component of the power required to rotate the foil in its pitching motion was actually negative in the mean, indicating that, at this phase angle, the fluid was doing work to help the motion.

To help understand these results, the scaling relations for the mean thrust and power generated by a heaving and pitching foil were developed by considering lift-based and added mass forces and moments, which were based on the relations for heaving or pitching foils developed by Floryan et al. [19]. These scaling relations described the experimental performance behavior well and indicated the need to increase the motion amplitudes (specifically pitch angle) while minimizing the peak angle of attack to increase thrust and efficiency.

The results of [8–10] on large-amplitude heaving and pitching foils lend confidence to the current conclusions; they use relatively large motions (h_0/c up to 0.75 and θ_0 up to 65 deg) as compared to the experiments described here while keeping the angle of attack small ($\alpha_0 \approx 20$ deg), leading to very high propulsive efficiencies: $\eta \approx 0.55$–0.8. For the present experiments on a teardrop airfoil, efficiencies of 45–50% are obtained over a large parameter space of motion amplitudes. Some cases display efficiencies as high as 60–75%, but the peak values are very sensitive to the drag on the foil, and so the foil profile is likely to be a crucial design parameter. Such considerations will be left for future study.

Appendix A: Complete Performance Results

Figures A1–A6 show the nondimensional input parameters (Strouhal number, trailing-edge amplitude to chord ratio, and peak angle of attack) and time-averaged output performance (thrust, power, efficiency) for all the phase offsets, frequencies, heave amplitudes, and pitch amplitudes tested (see Table 1).
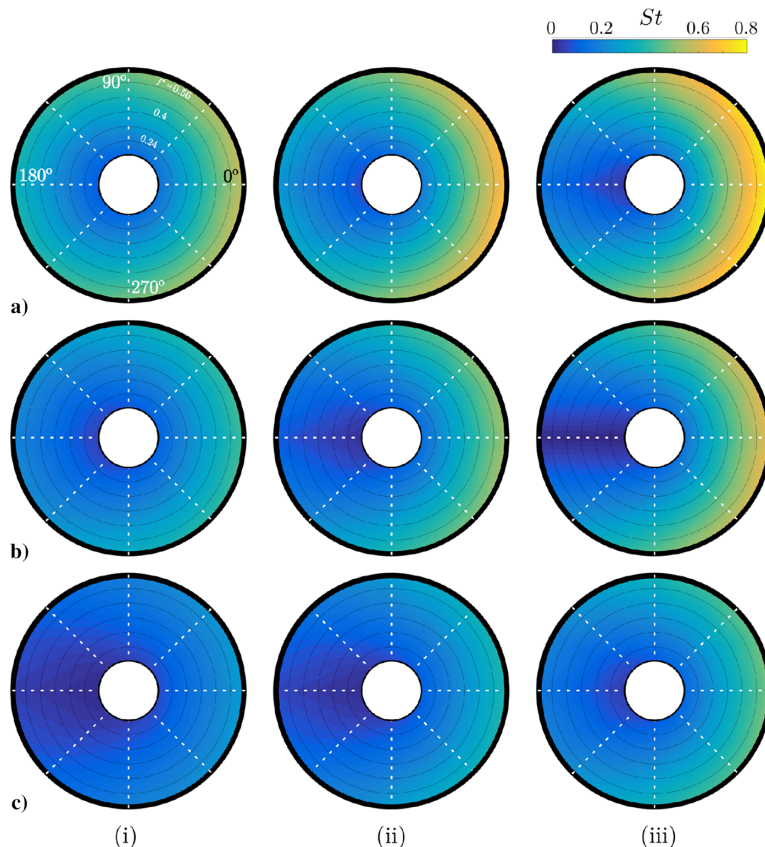

Fig. A1 Impact of phase offset (ϕ, azimuthal axis) and reduced frequency (f^*, radial axis) on Strouhal number for the following combinations of heave amplitudes: a) $h_0/c = 0.375$, b) 0.25, and c) 0.125; and pitch amplitudes i) $\theta_0 = 5$ deg, ii) 10 deg, and iii) 15 deg. The frequency increases radially outward, with lines marking levels at $f^* = 0.16, 0.24, \ldots, 0.64$.
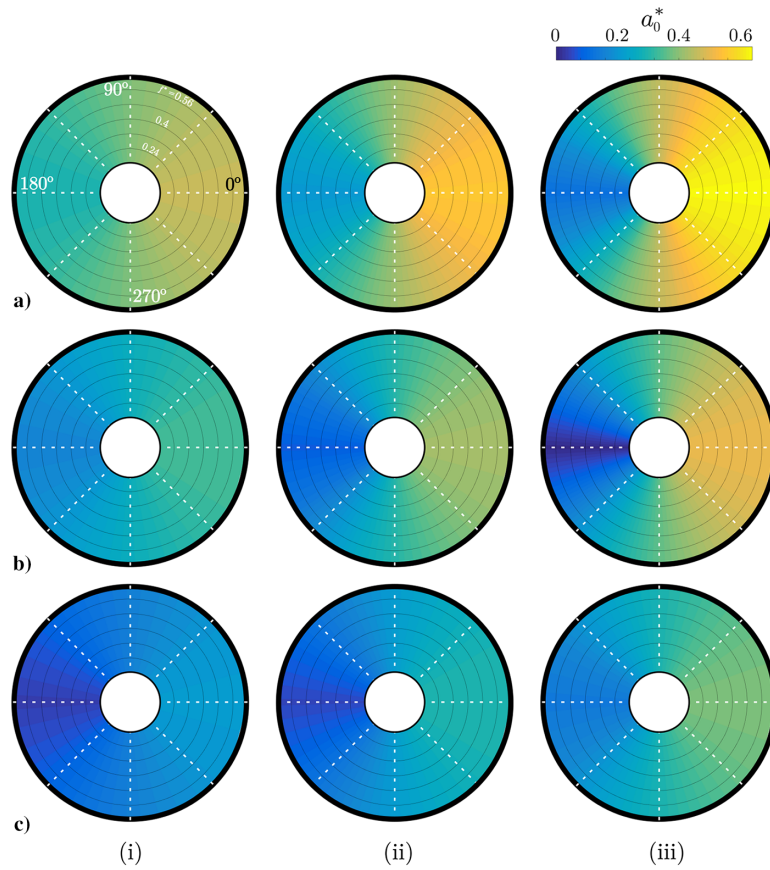
Fig. A2   Impact of phase offset (ϕ, azimuthal axis) and reduced frequency (f^*, radial axis) on the peak trailing-edge amplitude to chord ratio. Subfigures cases as in Fig. A1.

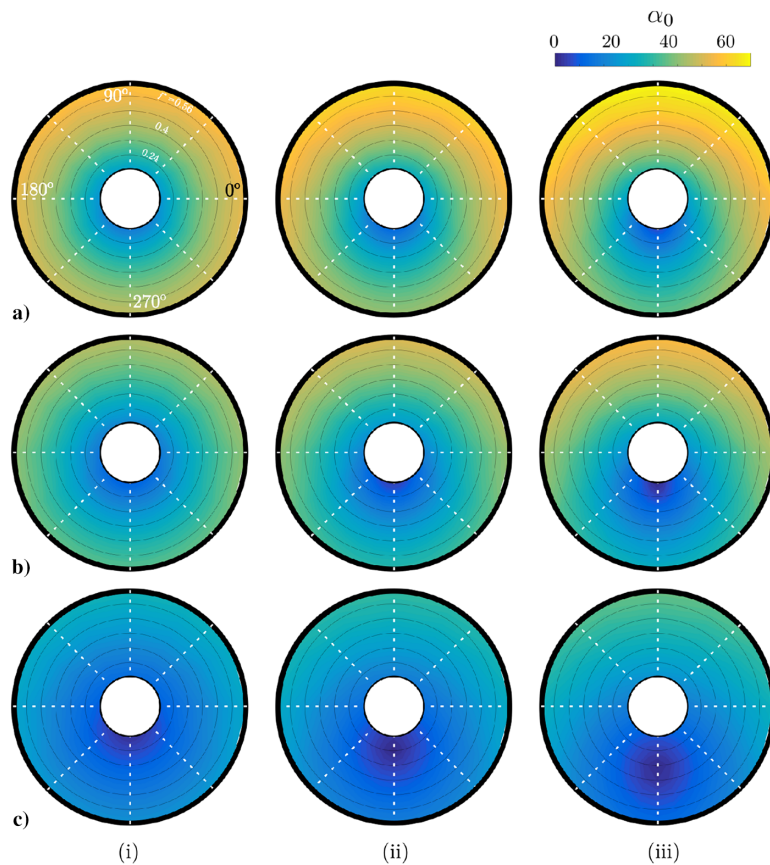**Fig. A3   Impact of phase offset (ϕ, azimuthal axis) and reduced frequency (f^*, radial axis) on the peak angle of attack. Subfigures cases as in Fig. A1.**
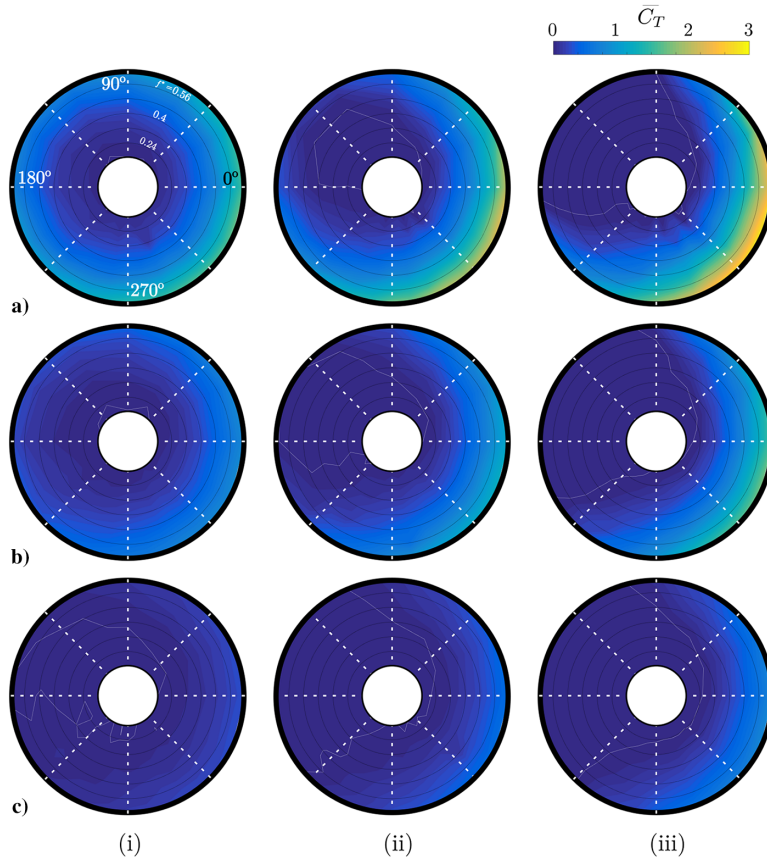
Fig. A4 Impact of phase offset (ϕ, azimuthal axis) and reduced frequency (f^*, radial axis) on the thrust coefficient. Subfigures cases as in Fig. A1.
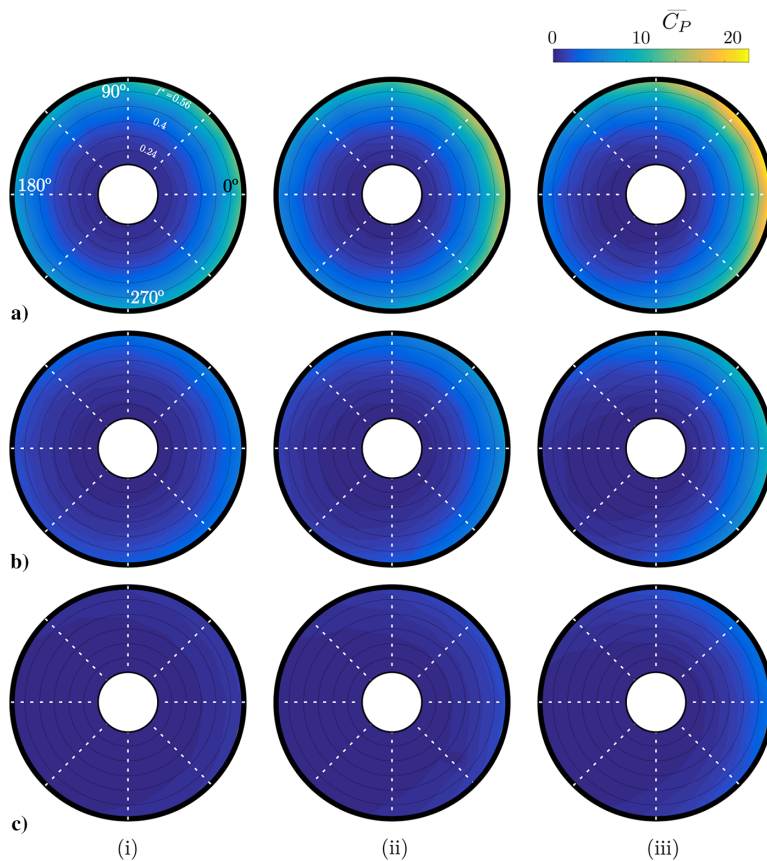

Fig. A5 Impact of phase offset (ϕ, azimuthal axis) and reduced frequency (f^*, radial axis) on the power coefficient. Subfigures cases as in Fig. A1.
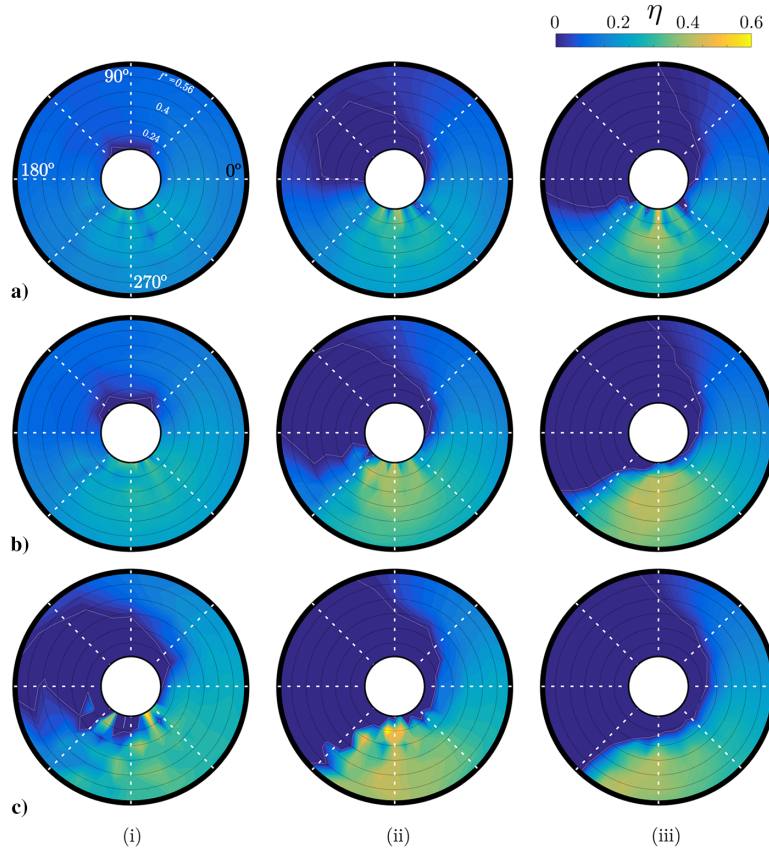
Fig. A6   Impact of phase offset (ϕ, azimuthal axis) and reduced frequency (f^*, radial axis) on the propulsive efficiency. Subfigures cases as in Fig. A1.

Appendix B: Foil Viscous Drag Assessment

As the foil becomes still ($f \to 0$), the viscous drag of the foil should depend on the mean projected area of the foil over the entire motion cycle. Accordingly, the drag should only be a function of the pitch amplitude and not a function of the heave amplitude. Figure B1 shows the drag coefficient as it varies with motion amplitude for heaving and pitching motions at three very low frequencies. The forces due to viscous drag are low; thus, the experiments are repeated 10 times each and the uncertainty bars on the symbols reflect the standard deviation of the data. Note that points at heave amplitudes $h_0 = 20$, 25, and 30 mm for a frequency of $f = 0.05$ Hz are removed because the linear actuator cannot operate smoothly at this combination of low frequency/high amplitude. The drag coefficient is clearly a function of the pitch but not the heave amplitude for steady motion.

Acknowledgments

References

[1] Sfakiotakis, M., Lane, D. M., and Davies, J. B. C., "Review of Fish Swimming Modes for Aquatic Locomotion," *IEEE Journal of Oceanic Engineering*, Vol. 24, No. 2, 1999, pp. 237–252.
doi:10.1109/48.757275

[2] Triantafyllou, M. S., Triantafyllou, G. S., and Yue, D. K. P., "Hydrodynamics of Fishlike Swimming," *Annual Review of Fluid Mechanics*, Vol. 32, No. 1, 2000, pp. 33–53.
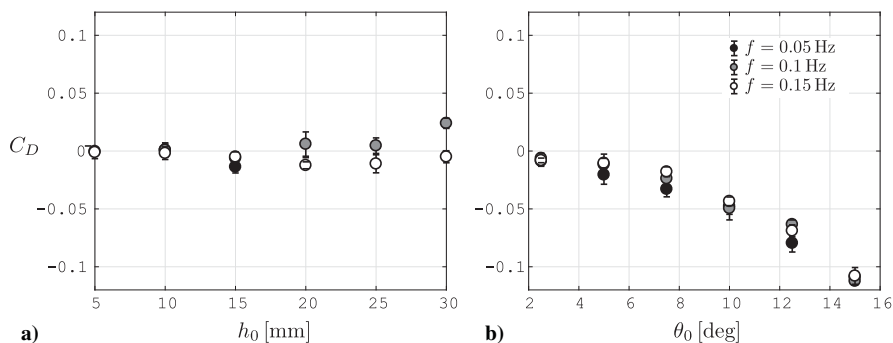doi:10.1146/annurev.fluid.32.1.33

Fig. B1   Drag coefficient as it varies with frequency and motion amplitude for a) heaving and b) pitching motions.

[3] Wu, T. Y., "Fish Swimming and Bird/Insect Flight," *Annual Review of Fluid Mechanics*, Vol. 43, No. 1, 2011, pp. 25–58.
doi:10.1146/annurev-fluid-122109-160648

[4] Lindsey, C. C., "Form, Function, and Locomotory Habits in Fish," *Fish Physiology*, edited by W. S. Hoar, and D. J. Randall, Vol. 7, Academic Press, New York, 1978, pp. 1–100.
doi:10.1016/S1546-5098(08)60163-6

[5] Lighthill, M. J., "Aquatic Animal Propulsion of High Hydromechanical Efficiency," *Journal of Fluid Mechanics*, Vol. 44, No. 2, 1970, pp. 265–301.
doi:10.1017/S0022112070001830

[6] Dickinson, M. H., "Unsteady Mechanisms of Force Generation in Aquatic and Aerial Locomotion," *American Zoologist*, Vol. 36, No. 6, 1996, pp. 537–554.
doi:10.1093/icb/36.6.537

[7] Von Ellenrieder, K. D., Parker, K., and Soria, J., "Flow Structures Behind a Heaving and Pitching Finite-Span Wing," *Journal of Fluid Mechanics*, Vol. 490, Sept. 2003, pp. 129–138.
doi:10.1017/S0022112003005408

[8] Anderson, J. M., Streitlien, K., Barrett, D. S., and Triantafyllou, M. S., "Oscillating Foils of High Propulsive Efficiency," *Journal of Fluid Mechanics*, Vol. 360, April 1998, pp. 41–72.
doi:10.1017/S0022112097008392

[9] Read, D. A., Hover, F. S., and Triantafyllou, M. S., "Forces on Oscillating Foils for Propulsion and Maneuvering," *Journal of Fluids and Structures*, Vol. 17, No. 1, 2003, pp. 163–183.
doi:10.1016/S0889-9746(02)00115-9

[10] Scherer, J. O., "Experimental and Theoretical Investigation of Large Amplitude Oscillation Foil Propulsion Systems," Tech. Rept. 662-1, Hydronautics, Inc., Laurel, MD, 1968.

[11] Kaya, M., and Tuncer, I. H., "Nonsinusoidal Path Optimization of a Flapping Airfoil," *AIAA Journal*, Vol. 45, No. 8, 2007, pp. 2075–2082.
doi:10.2514/1.29478

[12] Theodorsen, T., "General Theory of Aerodynamic Instability and the Mechanism of Flutter," NACA TR 496, 1949; also NACA TR ARR-1935, 1935.

[13] Garrick, I. E., "Propulsion of a Flapping and Oscillating Airfoil," NACA TR 567, 1937.

[14] Lighthill, M. J., "Large-Amplitude Elongated-Body Theory of Fish Locomotion," *Proceedings of the Royal Society of London, Series B: Biological Sciences*, Vol. 179, No. 1055, 1971, pp. 125–138.
doi:10.1098/rspb.1971.0085

[15] Chopra, M. G., "Hydromechanics of Lunate-Tail Swimming Propulsion," *Journal of Fluid Mechanics*, Vol. 64, No. 2, 1974, pp. 375–392.
doi:10.1017/S002211207400245X

[16] Chopra, M. G., and Kambe, T., "Hydromechanics of Lunate-Tail Swimming Propulsion. Part 2," *Journal of Fluid Mechanics*, Vol. 79, No. 1, 1977, pp. 49–69.
doi:10.1017/S0022112077000032

[17] Wu, T. Y., "Swimming of a Waving Plate," *Journal of Fluid Mechanics*, Vol. 10, No. 3, 1961, pp. 321–344.
doi:10.1017/S0022112061000949

[18] Katz, J., and Weihs, D., "Hydrodynamic Propulsion by Large Amplitude Oscillation of an Airfoil with Chordwise Flexibility," *Journal of Fluid Mechanics*, Vol. 88, No. 3, 1978, pp. 485–497.
doi:10.1017/S0022112078002220

[19] Floryan, D., Van Buren, T., Rowley, C. W., and Smits, A. J., "Scaling the Propulsive Performance of Heaving and Pitching Foils," *Journal of Fluid Mechanics*, Vol. 822, July 2017, pp. 386–397.
doi:10.1017/jfm.2017.302

[20] Sedov, L. I., *Two-Dimensional Problems in Hydrodynamics and Aerodynamics*, Interscience, New York, 1965, pp. 20–30.

[21] Floryan, D., Van Buren, T., and Smits, A. J., "Forces and Energetics of Intermittent Swimming," *Acta Mechanica Sinica*, Vol. 33, No. 4, 2017, pp. 725–732.
doi:10.1007/s10409-017-0694-3

[22] Van Buren, T., Floryan, D., Quinn, D., and Smits, A. J., "Nonsinusoidal Gaits for Unsteady Propulsion," *Physical Review Fluids*, Vol. 2, May 2017, Paper 053101.

[23] von Kármán, T., and Burgers, J. M., "General Aerodynamic Theory: Perfect Fluids," *Aerodynamic Theory, Vol. II, Div. E*, edited by W. F. Durand, Springer–Verlag, Berlin, 1934, pp. 280–310.

[24] Triantafyllou, G. S., Triantafyllou, M. S., and Grosenbaugh, M. A., "Optimal Thrust Development in Oscillating Foils with Application to Fish Propulsion," *Journal of Fluids and Structures*, Vol. 7, No. 2, 1993, pp. 205–224.
doi:10.1006/jfls.1993.1012

[25] Van Buren, T., Floryan, D., Wei, N., and Smits, A. J., "Flow Speed has Little Impact on Propulsive Characteristics of Oscillating Foils," *Physical Review Fluids*, Vol. 3, No. 1, Jan. 2018, Paper 013103.

[26] Liu, T., Wang, S., Zhang, X., and He, G., "Unsteady Thin-Airfoil Theory Revisited: Application of a Simple Lift Formula," *AIAA Journal*, Vol. 53, No. 6, 2015, pp. 1492–1502.

[27] Alexander, R. M., *Principles of Animal Locomotion*, Princeton Univ. Press, Princeton, NJ, 2003, pp. 249–250.

P. Givi
Associate Editor